Chinese Chemical Letters 35 (2024) 108831

Contents lists available at ScienceDirect

Chinese Chemical Letters

journal homepage: www.elsevier.com/locate/cclet

Circularly polarized luminescence switch based on a photochromic europium(III) helicate derived coordination polymer

Mei Li[a], Yanyan Zhou[a], Jingya Li[b], Wenru Huang[a], Zhiwei Yao[a], Yuying Li[a], Ting Gao[a], Pengfei Yan[a,*], Hongfeng Li[a,*]

[a] Key Laboratory of Functional Inorganic Material Chemistry, Ministry of Education, School of Chemistry and Materials Science, Heilongjiang University, Harbin 150080, China
[b] State Key Laboratory of Baiyunobo Rare Earth Resource Researches and Comprehensive Utilization Institution, Baotou 014030, China

ARTICLE INFO

Article history:
Received 29 May 2023
Revised 17 July 2023
Accepted 23 July 2023
Available online 26 July 2023

Keywords:
Chiroptical switches
Coordination polymer
CPL
Anti-counterfeiting
Logic gate

ABSTRACT

Chiroptical switches based on circularly polarized luminescence (CPL) have shown the promising applications in advanced information technologies. Herein, a pair of lanthanide coordination polymer enantiomers $[Eu_2(L^R)_3(BTFPO)_2]_n$ and $[Eu_2(L^S)_3(BTFPO)_2]_n$ with light-regulated CPL property are designed, which are assembled by a chiral binuclear triple-stranded Eu^{3+} helicates $[Eu_2(L^{R/S})_3]$ coordinated with two photochromic triphenylphosphine oxides (BTFPO). Upon the alternative UV and 526 nm light irradiation, the complexes show the reversible photochromism, PL and CPL responses. Notably, the luminescence dissymmetry factor, g_{lum} of $^5D_0 \rightarrow {}^7F_1$ (591 nm) transition shows an obvious increase from 0.19 to 0.29 before and after 275 nm light irradiation. Additionally, the emission from Eu^{3+} center is not completely quenched in closed-ring state due to the low photocyclization ($\Phi_{o\text{-}c}$) quantum yield of the polymer. The partial maintenance of emissive intensity is of essential importance for the monitor of CPL signal. More importantly, the CPL photo-switching property of the complexes in solid hybrid film is maintained, and still displays the enhanced CPL emission in photostationary state. Further, the potential applications of the doping film in logic gate and anti-counterfeiting were investigated.

Photoswitches have attracted much interest because of their promising applications in optical storage [1,2], logic gate [3,4], information encryption [5–7] and sensors [8–10]. Obviously, if the photoswitches enable to output much more optical signals through one light stimulation, it will significantly improve their capabilities on information processing. The introduction of chiroptical signals (such as CPL and CD) is an alternative method to increase the dimension of optical outputs. In comparison with the extensively reported CD-based chiroptical switches [11,12], the counterparts based on circularly polarized luminescence (CPL) were seldom reported [13,14]. This is because the luminescence dissymmetry factor (g_{lum}), which represents the degree of preference of left- or right-circularly polarized light over the other, is usually very small (often $g < 0.1$, $g_{max} = 2$) [15]. This disadvantage extremely limits their applications as CPL switch.

Diarylethenes (DAEs) and their derivatives are regarded as the most widely used photo-responsive components in chiroptical switches [16,17]. Recently, a few examples of CPL switches based on diarylethene (DAEs) have been reported [18]. For instance, Akagi reported the first light stimuli-responsive CPL material based on a diarylethene modified polymer [19]. A more recent example is that reported by Liu and Zhang [20], where a "on-off" CPL switch constructed from supramolecular gel is prepared by virtue of photoisomerization of diarylethene. However, how to resolve the issue of the low g_{lum} value of materials is still a challenge for the further development of CPL switch.

Among CPL materials, the lanthanide complexes usually showed the obviously higher g_{lum} values (typically with $g_{lum} = 10^{-2}-1$) compared to organic luminophores [21,22]. This is because the partial transitions of Ln^{3+} ion possess the magnetic dipole transition feature. Thus, the employment of chiral lanthanide complexes to fabricate CPL switch is undoubtedly a feasible strategy. In this aspect, our group have reported a few examples of CPL switch based on the DAEs modified lanthanide helicates [23–25]. In these chiral helicates, the photoisomerization of DAEs result in the variations of the helical chirality of the assemblies, and subsequently realize the modulation to CPL (g_{lum} values).

To further improve g_{lum} and the magnitude of photomodulation, we herein synthesized a pair of enantiomers of lanthanide coordination polymer, which are comprised of the chi-

* Corresponding authors.
E-mail addresses: Yanpf@vip.sina.com (P. Yan), lihongfeng@hlju.edu.cn (H. Li).

https://doi.org/10.1016/j.cclet.2023.108831
1001-8417/

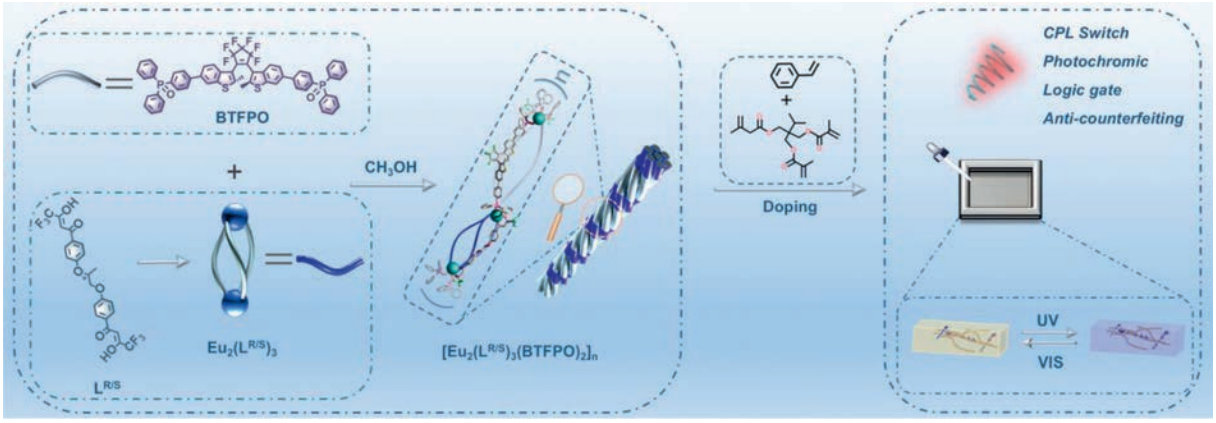

Scheme 1. Synthetic routes of lanthanide coordination polymer $[Eu_2(L^{R/S})_3(BTFPO)_2]_n$ and the preparation of doping film.

ral binuclear Eu^{3+} helicates and a diarylethene modified triphenylphosphine oxide as ancillary ligand. In comparison with our previously reported photochromic ligands that combined DAEs and chiral element in one ligand, the usage of photochromic ancillary ligand strategy provides a "master key" approach, which can be used to regulate the CPL of all the chiral lanthanide complexes, once they coordinate with Ln^{3+} ion. In two complexes, each two bidentate phosphine oxide ancillary ligands bridge two helicates to form a 1-D chain liked coordination polymer (Scheme 1). The optical and chiroptical analyses show that the complex enables to undergo a reversible CPL light modulation, and accompanied with a remarkable variation of g_{lum} value from 0.19 (open-ring state) to 0.29 (photostationary state (PSS)). It is suggested that the remarkable variation of g_{lum} value should arise from the synergetic chirality amplify effect brought by the formation of 1-D supramolecular chain. A similar chirality amplify effect can often be observed in chiral supramolecular assemblies [26,27]. Additionally, we also examine the CPL switching performance of complexes in doping film. The maintenance of photochromic and light-regulated CPL properties in film encouraged us to further develop the usage of complexes in logic gate and anti-counterfeiting.

The synthetic procedure of the photochromic diarylethene ancillary ligand, BTFPO is shown in Scheme S1 (Supporting information). The BTFPO is comprised of two triphenylphosphine oxides (TPPO) bridged by a well-known photochromic diarylethene, 1,2-bis(2-methylbenzo[*b*]-thiophen-3-yl)hexafluorocyclopentene (BTF6) [28]. It was synthesized by Suzuki coupling of the triphenyloxyphosphonborate ester with diiodo-BTF6 catalysed by $Pd(PPh_3)_2Cl_2$. The diiodo-BTF6 was prepared according to the reported methods [29]. The corresponding intermediates and ancillary ligands were confirmed by ^1H NMR and MS (Figs. S1−S7 in Supporting information). The triple-stranded helicates, $Eu_2(L^R)_3$ and $Eu_2(L^S)_3$ were prepared by the self-assembly of $Eu(OTf)_3$ with our previously reported chiral (*R/S*)−1,2-propanediol derived bis-β-diketonate ligand ($L^{R/S}$) in methanol [30]. The coordination polymer $[Eu_2(L^{R/S})_3(BTFPO)_2]_n$ was prepared by further assembly of the helicates $Eu_2(L^{R/S})_3$ with BTFPO in a 1:2 ratio in refluxed methanol (Scheme 1). ESI-MS first affirms the successful preparation of triple-stranded helicate (Fig. S9 in Supporting information), which displays the molecular ion peak of the positive charged species, $[Eu_2(L^{R/S})_3 + H]^+$ at m/z = 1811.0308. However, it is known that the analysis towards coordination polymer by MS is difficult due to the huge formula weight. Fortunately, the mass fragments generated during ionization process of polymer can offer the valuable information to estimate the formation of the expected structure. As shown in Fig. 1a, the fragment peaks attributed to the $[Eu_2(L^R)_3 + 2BTFPO + H]^+$ at m/z = 3868.5624 was clearly observed (Fig. 1a),

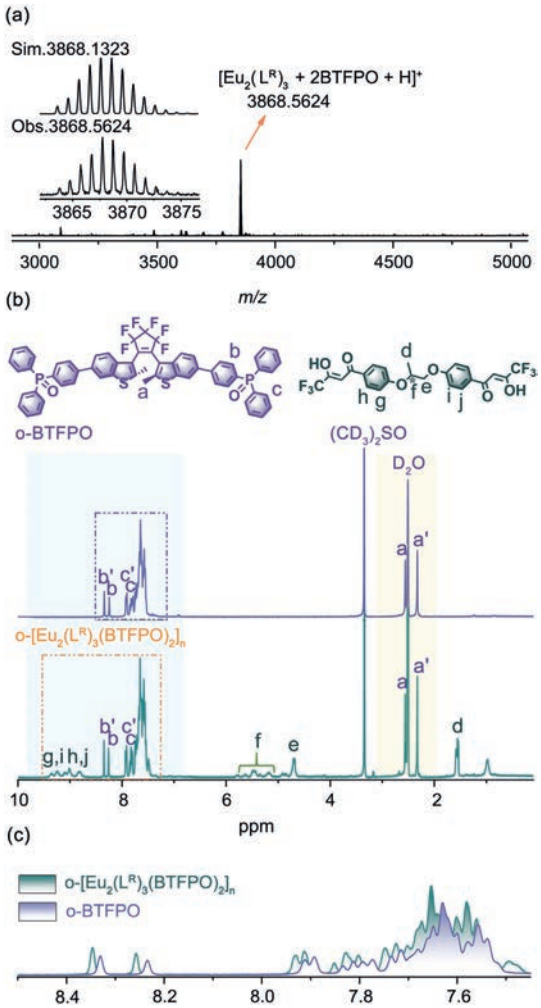

Fig. 1. (a) ESI-MS spectrum of $[Eu_2(L^R)_3(BTFPO)_2]_n$ with the inset representing the simulated (Sim.) and observed (Obs.) isotopic distributions. (b) ^1H NMR spectra (400 MHz) of o-BTFPO (purple line), and the polymer o-$[Eu_2(L^R)_3(BTFPO)_2]_n$ (olive line) in DMSO–d_6. (c) The overlapped ^1H NMR spectra of o-BTFPO (purple line) and o-$[Eu_2(L^R)_3(BTFPO)_2]_n$ (olive line) in DMSO–d_6.

which provides valuable information to deduce the composition of the coordination polymer.

The corrected 1:2 stoichiometric ratio of $Eu_2(L^{R/S})_3$ to BFTPO in chemical formula $[Eu_2(L^{R/S})_3(BTFPO)_2]_n$ can be verified by ^1H NMR of the complex (Fig. 1b). The integration ratio of methyl

protons in BTFPO (Ha and Ha′) to those in helicates (Hd) is 4:3, which is in accordance with the expected polymer composition of $[Eu_2(L^{R/S})_3(BTFPO)_2]_n$. Moreover, the spectral shift of BTFPO in free ligand compared to that in complex also supports the coordination of BTFPO to Ln^{3+} ion (Fig. 1c). Additionally, the peaks of methyl protons, Ha and Ha′, corresponding to parallel (*p*) and antiparallel (*ap*) conformations, are sharp and well distinguishable. From their integration area, the ratios of *ap*- and *p*-conformers of BTFPO in free ligand and the complexes are estimated to be 4.9:5.1 and 4.7:5.3, respectively. It is well known that only the *ap*-conformation could perform photoisomerization.

To obtain the exact structure, several methods have been tried to grow single crystals of the complex, but all the efforts failed. Thus, herein, we resorted to a semiempirical molecular mechanics modeling fabricated by the LUMPAC 3.0 software with a Sparkle/AM1 model to optimize the possible structure. On the basis of our previously reported quadruple-stranded helicate, $Eu_2(L^R)_4$, a triple-stranded helical structure $Eu_2(L^R)_3$ was first optimized. With this structure, a polymer fragment comprised of two helicates and two BTFPO was successfully optimized (Fig. S10 in Supporting information). In this model, we observed that the helicate adopts *M*-helical conformation, and induces the antiparallel BTFPO to generate *P* conformation.

BTF6 and its derivatives as well-known photochromic compounds have been widely used in areas of optical switch, storage and cell imaging due to their high thermal stability and photochromic conversion efficiency [31,32]. Herein, a new photochromic molecule, BTFPO is designed by BTF6 covalently linked with two triphenylphosphine oxides (TPPO). It is expected that this compound will remain the well photochromic performance in coordination polymer. Thanks to the multiple aryl groups and nonplanar structure of BTFPO, the free ligand and its corresponding complexes both exhibit good solubility in solvent. The solution concentration of polymer can reach up to 10^{-3} mol/L (estimated by helicate) in THF, which provides the possibility to assess the photophysical properties of the polymer in solution.

Herein, we first compared the photochromic performance of the free BTFPO and $[Eu_2(L^{R/S})_3(BTFPO)_2]_n$ in THF. The UV−vis spectra of the free BTFPO and the complex before and after photoisomerization are shown in Fig. S18 (Supporting information). In open-ring form, the absorbance of BTFPO locates at UV band with $\lambda_{max} = 292$ nm. Upon irradiating with 275 nm UV light, two new bands with maxima absorbances at 384 and 550 nm appear, and resulting in the color of solution from colourless to purple. After irradiation for 15 min, the free BTFPO reaches a photostationary state (insert of Fig. S18a in Supporting information), indicating the presence of partial photocyclization of BTFPO from an open-ring (o-BTFPO) to closed-ring (c-BTFPO) form. The reversal photoisomerization is realized by exposure to 526 nm LED light for 80 s (Fig. S12 in Supporting information). Based on the variation plot of absorbance *versus* time, the photocyclization ($\Phi_{o\text{-}c}$) and photocycloreversion ($\Phi_{c\text{-}o}$) quantum yields are calculated to be 4.6% and 31.2%, respectively. From the integration area of Ha and Ha′ in ^{1}H NMR, the conversion ratio (α_{PSS}) of o-BTFPO to c-BTFPO in photostationary state is calculated to be 3.8% (Fig. S11 in Supporting information).

The absorbance variation of the coordination polymer in THF is shown in Fig. S18b (Supporting information). In open-ring state of BTFPO, the complex $[Eu_2(L^R)_3(BTFPO)_2]_n$ presents a main band with a maximum absorbance at 326 nm and a shoulder at 295 nm, which is ascribed to the characteristic π–π transition of bis-β-diketone (L) and the absorbance of BTFPO, respectively. Meanwhile, upon irradiation with UV light at 275 nm, the colourless solution of polymer in open-ring form gradually turns to purple, and followed with the presence of two new bands at 386 and 551 nm. In comparison with the free BTFPO, the time reaching to photostationary state is delayed to 20 min (insert of Fig. S18b in Supporting information), and displays the relative decrease of absorbance. ^{1}H NMR analysis shows that the conversion ratio of photoisomerization of BTFPO in complex decreases to 2.9% (Fig. S14 in Supporting information). Additionally, the photocyclization ($\Phi_{o\text{-}c}$) quantum yields lower to 0.55%, while the photocycloreversion ($\Phi_{c\text{-}o}$) does not present the obvious decrease, remaining at 30.1%. These results indicate that the formation of coordination polymer markedly affects the photoisomerization of BTFPO. Although the presence of the low closed-ring conversion ratio, the coordination polymer still exhibits excellent reversibility and stability (Figs. S15−S17 in Supporting information).

The typical feature of the photochromic compounds is their existence of the markedly spectral shift under the alternative light stimuli. For lanthanide complexes, the luminescence from Ln^{3+} ion depends on the effective energy transfer from ligand to emissive energy level of metal center. Thus, the variation of energy level caused by photoisomerization will certainly influence the luminescence from the complexes. However, the absolute luminescence quenching also indicates the simultaneous turn-off of PL and CPL emission, which makes the switch relying on CPL signals lose the advantage of chiroptical regulation.

Thanks to the low photoisomeric efficiency, the polymer reported here remains the enough emission intensity after photocyclization. As shown in Fig. 2a, the complex shows the characteristic emission of Eu^{3+} ions at 591, 611, 648, and 699 nm, corresponding to $^5D_0 \rightarrow {}^7F_J$ ($J = 1$–4) transitions, respectively. In comparison with the open-ring form, the emission intensity in photostationary state decreased by 76%. The relative photophysical parameters are listed in Table S1 (Supporting information). The data show that the luminescence quantum yields (QYs) of the polymer in open- and closed-ring form are 20.5% and 5.6%, respectively. The about 5% total emission efficiency in photostationary state is enough to satisfy the sensitivity of the current commercial detector.

For lanthanide complexes, the highly effective luminescence depends on the energy level match between the triplet state (T_1) of ligand and the excited state of Ln^{3+} ion. The triplet state energy level can be estimated from the phosphorescence spectrum of the corresponding Gd^{3+} complex. By referring to the high energy emission edge of $Gd_2(L^R)_3(CH_3OH)_2$, the T_1 of L is calculated to be 22,200 cm^{-1} (Fig. S21 in Supporting information), which is higher than the $^5D_0$ energy level (17,500 cm^{-1}) of Eu^{3+} ion. The ΔE (T_1 – $^5D_0$ = 4700 cm^{-1}) satisfies the suggested energy difference, $\Delta E > 2500$ cm^{-1} for a highly effective energy transfer process [33]. In open-ring form of $[Gd_2(L^R)_3(BTFPO)_2]_n$, the phosphorescence spectrum is in accordance with that of $Gd_2(L^R)_3(CH_3OH)_2$. It indicates that the phosphorescent emission from BTFPO is probably covered by the emission of L. In the case of closed-ring form, a new band presents at the low energy spectral region with high energy emission edge at 15,197 cm^{-1} (620 nm), which is lower than $^5D_0$ energy level (17,500 cm^{-1}) of Eu^{3+} ion, indicating the presence of an invalid energy transfer from BTFPO to Eu^{3+} ion (Fig. S22 in Supporting information). Conversely, the T_1 of BTFPO can accept the energy from $^5D_0$ of Eu^{3+} and T_1 (22,200 cm^{-1}) of L. This result can well explain the partial quenching from Eu^{3+} center. The phosphorescence decay curves of the corresponding $[Gd_2(L^R)_3(BTFPO)_2]_n$, are shown in Fig. S23 (Supporting information), and the proposed energy transfer processes of o-$[Eu_2(L^R)_3(BTFPO)_2]_n$ and c-$[Eu_2(L^R)_3(BTFPO)_2]_n$ are summarized in Scheme S2 (Supporting information).

Because of the introduction of point chirality at the spacer of $L^{R/S}$, the chirality of the complex in ground and excited states, and their chiroptical properties regulated by light stimuli are expected. Fig. 2b displays the mirror-image CD curves of the polymers before and after photoisomerization. In UV band, the variations of CD signals are negligible in open-ring and photostationary states. It indi-

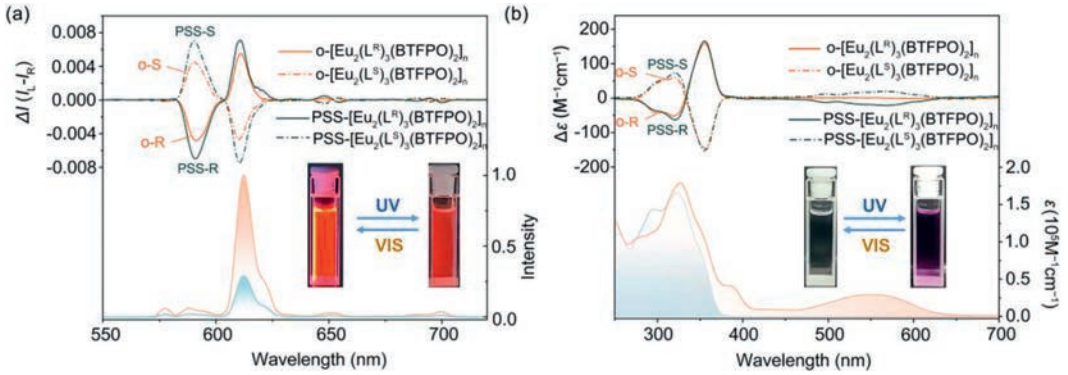

Fig. 2. (a) UV−vis absorption (lower curve, right axis) and CD spectra (upper curves, left axis). (b) PL (lower curve, right axis) and CPL spectra (upper curves, left axis) $[Eu_2(L^R)_3(BTFPO)_2]_n$ and $[[Eu_2(L^S)_3(BTFPO)_2]_n$ in the open-ring and photostationary states ($c = 1 \times 10^{-5}$ mol/L, THF).

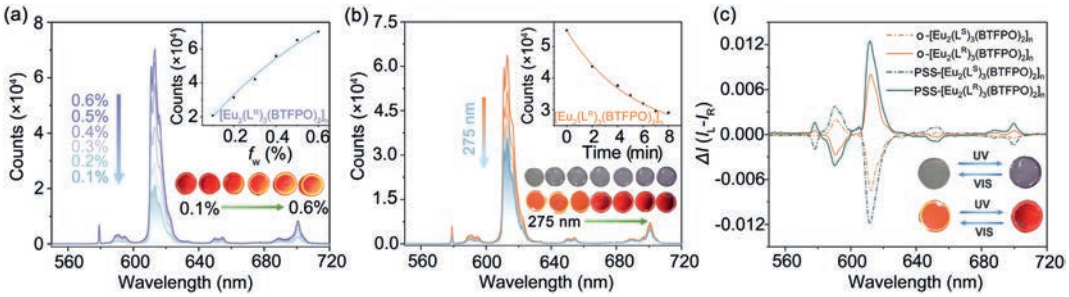

Fig. 3. (a) Emission spectra of hybrid films with doping levels of 0.1%−0.6%. (b) Emission spectra of hybrid films with doping levels of 0.6% after exposure to 275 nm UV with 1.0 min interval time. (c) CPL spectra comprised of polymer film with the open-ring and photostationary states (doping amount = 0.6%).

cates that photocyclization does not lead to the perceptible change of supramolecular chirality of the helicate. However, the presence of exciton coupling in this band offers useful information to estimate the supramolecular chirality of the helicate. A positive exciton coupling for $[Eu_2(L^R)_3(BTFPO)_2]_n$ indicates the presence of a Λ configuration around Eu^{3+} ion and an *M*-helical conformation for the helicate. This result is in accordance with the optimized structure from LUMPAC calculation. While in the visible spectral region, the new mirror-image Cotton curves attributed to close ring c-BTFPO are observed, indicating the presence of an effective chirality transfer from helicate to BTFPO.

The excited state chirality from Eu^{3+} ion is monitored by CPL spectrum. Fig. 2a shows the mirror-image CPL spectra of the enantiomeric polymer in the corresponding emission bands of Eu^{3+} ion, in which $^5D_0 \rightarrow {}^7F_1$ (591 nm) and $^5D_0 \rightarrow {}^7F_2$ (611 nm) transitions show the relatively large ΔI. Thanks to the magnetic dipole transition feature, the g_{lum} value reaches up to 0.19 for $^5D_0 \rightarrow {}^7F_1$ transition in open-ring state. Notably, in photostationary state, the ΔI displays the obvious enhance, with g_{lum} value increasing to 0.29, although the total emission intensity is lower than the initial state. Combining the effective luminescence (QYs, 20.5% and 5.6% in open- and close-state) and the large $\Delta g_{lum} = 0.1$, this coordination polymer shows the promising potential as CPL switch.

As photochromic materials, their performances in solid state are of essential importance. Polymer, such as PMMA and PS, are the extensively used matrix for the preparation of luminescent doping film [34,35]. In the process of photoisomerization of DAEs, the matrix must provide enough space to fit the variation of molecule volume arising from photocyclization. In view of the case, we prepared a copolymerization film by employing styrene and trihydroxymethylpropyl trimethylacrylate (TMPTMA, Scheme 1) as monomers. The tripodal structure of TMPTMA enables the film to form a 3D framework with a large cavity inside.

After the successful preparation of polymer film, we first examine the doping level of the complexes as considering their limited solubility in matrix. The doping test shows the maximal doping amounts of the complexes in matrix is 0.6%. Whereafter, the effect of the doping level on emission intensity was investigated. As shown in Fig. 3a, the emission intensity gradually increases with the increase of doping concentration from 0.1% to 0.6%.

To facilitate the luminescent monitor, the 0.6% doping film was selected as an example to study the photochromic and CPL properties. Under 275 nm UV irradiation, this film displays the gradually deepened color change from colourless to purple (Fig. 3b, insert), and accompanying with the decrease of emission intensities. After 8 min irradiation, the photocyclization reaction reaches to photostationary state with the intensity dropping to 50% of initial state. Notably, the photoisomeric time is shorter than that of complex in solution (about 20 min.). The shortened time should arise from the space-restricted effect of the cavity in film, which probably shorten the distance between two reaction carbon atoms, thus facilitating the photocyclization reaction.

Importantly, CPL emission variation of the complex in hybrid film is also observed under the alternative UV and visible light irradiation (Fig. 3c). Similar to the case in solution, the film also presents CPL enhancement in photostationary states with the $|g_{lum}|$ values at 590 nm increasing from 0.064 to 0.12. Notably, the ΔI attributed to $^5D_0 \rightarrow {}^7F_1$ (591 nm) transition displays the relative decrease compared to $^5D_0 \rightarrow {}^7F_2$ (612 nm) transition, which is different from the case in solution. The other difference is that the g_{lum} values at 612 nm present a markable increase from 10^{-3} (0.003) in solution to 10^{-2} (0.058) in film. In fact, for most of Eu^{3+} complexes, 10^{-2} order of magnitude of the g_{lum} value is difficult to achieve for the $^5D_0 \rightarrow {}^7F_2$ (612 nm) transition due to their electric dipolar transition feature. Thus, this band as monitoring wavelength is also accessible (Table S2 in Supporting information).

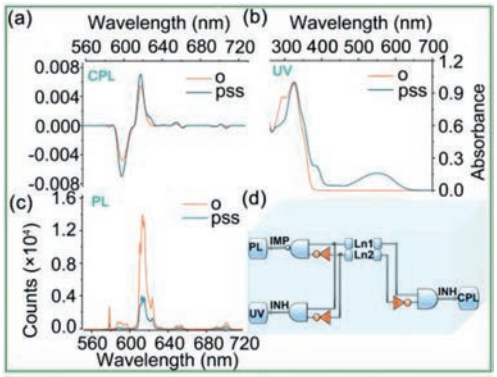

Input		Output		
		INH	IMP	INH
I_1 (275 nm)	I_2 (526 nm)	O_{CPL}	O_{PL}	O_{UV}
0	0	0	1	0
1	0	1	0	1
0	1	0	1	0
1	1	0	1	0

Fig. 4. The symbolic representation and truth table of the logic circuit. The two trigger wavelengths are denoted as input, I_1 (275 nm) and I_2 (526 nm). The output is defined as O_{CPL} (CPL signal at 591 nm) (a), O_{UV} (UV signal at 551 nm) (b), O_{PL} (PL signal at 611 nm) (c) and logic circuit (d).

In view of the multiple light stimuli response of the complexes, their potentials as advanced switching materials that is used in logic gate and anti-counterfeiting are developed [36]. Because the optical outputs of the films, such as UV, CD, PL and CPL, can be alternatively modulated by UV (λ = 275 nm) and green light (λ = 526 nm), thus the logic gates relying on these signals were fabricated. First, the input and output conditions should be defined to complete the corresponding logic design. Here, the UV wavelength at 275 nm is employed as input signal 1, named as "In1", while the green light with 526 nm wavelength is defined as input signal 2, named "In2". As the material not being stimulated by light, the logic inputs "In1" or "In2" are both regarded as "0", while the "1" indicates that the "In1" or "In2" is turned on.

Because of the same variation tendency of UV and CD spectra, their logic relationships are also the same. Thus, here we selected the UV signal as one logic output, and named as O_{UV}. The logic outputs of "0" and "1" of O_{UV} are defined by monitoring the absorbance at 551 nm ($A > 0$, $O_{UV} = 1$; $A = 0$, $O_{UV} = 0$). In the case of PL (O_{PL}) and CPL (O_{CPL}) as output signals, the emission intensity in photostationary state (λ_{em} = 611 nm) of PL and the initial g_{lum} value of CPL (λ_{em} = 591 nm) are defined as "0", while their corresponding increases are defined as logic output "1". With these logic relationships and the corresponding definitions, two kinds of logic gates named INHIBIT and IMPLICATION based on O_{UV}, O_{PL} and O_{CPL} are fabricated as shown in Fig. 4.

On the other hand, combination of photochromism and light-regulated CPL properties, the complexes show the potential combination of photochromism and light-regulated CPL properties, the complexes show the potential application in anti-counterfeiting. Herein, we prepared the letters "C", "P" and "L" films with the Eu^{3+} and Gd^{3+} complexes, $Eu_2(L^R)_3(BTFPO)_2]_n$, $[Eu_2(L^S)_3(BTFPO)_2]_n$, racemic $[Eu_2(L^{R/S})_3(BTFPO)_2]_n$ and $[Gd_2(L^R)_3(BTFPO)_2]_n$ as dopants. With these letters, we designed a simple matrix to discuss the possibility of the hybrid film for advanced anti-counterfeiting (Fig. 5a). In this matrix, the encrypted information can be decrypted in UV, PL and CPL modes. Further, the complete decryption need simultaneously satisfy the following three decryption conditions: (1) All the letters in matrix turn to purple under UV 275 nm irradiation, which can be determined by naked eyes or UV detector (Fig. 5b); (2) under 375 nm excitation light, the colourless letters (open-ring state) in cross line emit the bright red light, while the four let-

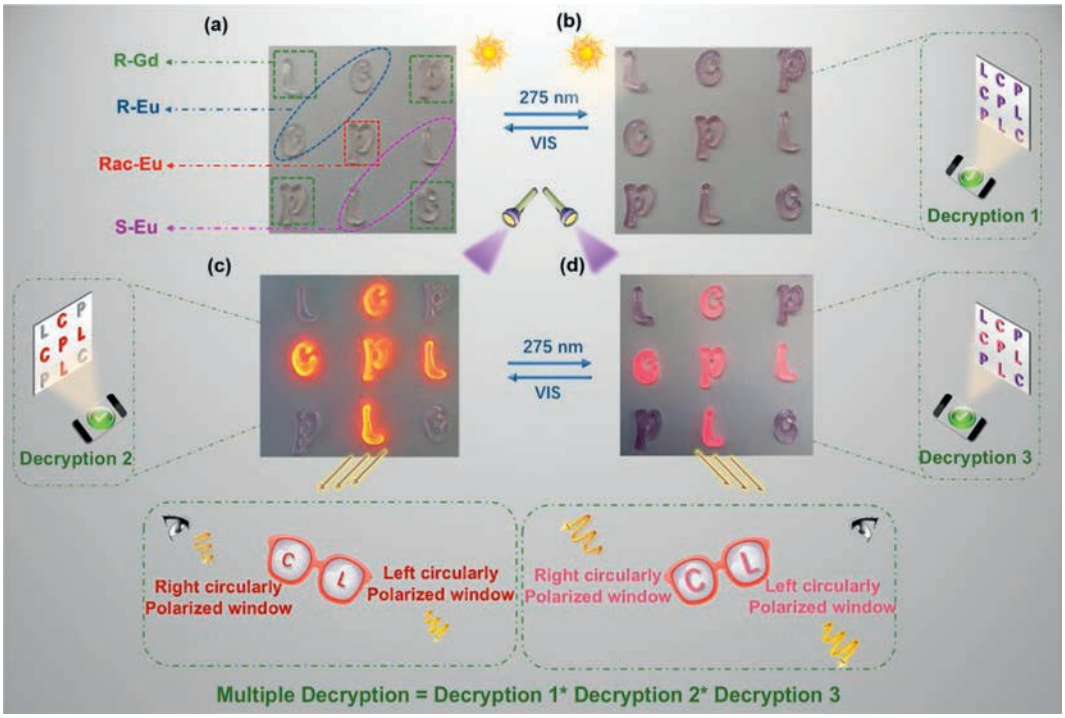

Fig. 5. Advanced information encryption and decryption based on a matrix comprised of doping film letters, "C", "P", "L". The letters in corner doped with $[Gd_2(L^R)_3(BTFPO)_2]_n$, letters "C" in cross line doped with $Eu_2(L^R)_3(BTFPO)_2]_n$, letters "L" in cross line doped with $Eu_2(L^S)_3(BTFPO)_2]_n$, letters "P" in cross line doped with rac-$[Eu_2(L^{R/S})_3(BTFPO)_2]_n$. Photos of all the letters in open-ring state (a, c) and photostationary state (b, d) under daylight and 365 nm irradiation, respectively.

ters in corner are not luminescent; meanwhile the letters "C" with left circularly polarized emission and "L" with right circularly polarized emission can be distinguished by left- or right-polarizing filters (Fig. 5c); (3) in the photostationary state, the letters on corner are purple and non-luminescent, but the enhanced CPL emission from letters "C" and "L" will be more easily distinguished by the polarizing filters (Fig. 5d). Compared with the conventional fluorescence anti-counterfeiting, such a matrix with the integration of UV, PL and CPL is endowed with multiple security features. This experiment demonstrates that the materials are suitable to realize the high-end anti-counterfeiting or information encryption.

In summary, this work reports the first example of a CPL photo-switch constructed from the lanthanide coordination polymer. Upon the alternative UV and green light irradiation, the complexes show the reversible light regulated UV, PL and CPL switchable properties in solution and in solid hybrid film. There are two advantages for the coordination polymer as excellent CPL optical switch: (1) The incomplete luminescence quenching of complexes in photostationary state. The relative high luminescence quantum yield is the precondition for the CPL signal to be monitored. Compared to the conventional fluorescence switch relying on emission quenching, the partial maintenance of luminescence can ensure the CPL signals in open- and close-ring state to be detectable; (2) The relatively large g_{lum} and the enhanced CPL in photostationary state. The $|g_{lum}|$ values of the complexes at 591 nm reach to 0.19 in colourless open-ring state, a relatively high value in lanthanide CPL materials. In photostationary state, this value increases to 0.29, the markable variation of $\Delta|g_{lum}| = 0.1$ ensures the determination to CPL signal to be facile and more correct. In fact, the two above aspects benefit from the formation of coordination polymer, which, on one hand, restricts the photocyclization of BTFPO, and resulting in the low $\Phi_{o\text{-}c}$ and the relatively high luminescence quantum yield. On the other hand, the chirality amplified effect caused by supramolecular assembly ensure the large $|g_{lum}|$ values of the polymer in open- and closed-ring state. Finally, the excellent photo-modulated chiroptical properties of the doping film demonstrate their potentials as photo-switching materials that used in logic gate and anti-counterfeiting.

Declaration of competing interest

The authors declare that they have no known competing financial interests or personal relationships that could have appeared to influence the work reported in this paper.

Acknowledgments

This work was financially supported by the National Natural Science Foundation of China (Nos. 52273263, 52203219, 51872077 and 52073080), Science and Technology Plan of Inner Mongolia Autonomous Region (No. 2020GG0164), Scientific Research Project of Basic Scientific Research Operating Expenses of Colleges and Universities in Heilongjiang Province (Nos. 2021-KYYWF-0029 and 2021-KYYWF-0041).

Supplementary materials

Supplementary material associated with this article can be found, in the online version, at doi:10.1016/j.cclet.2023.108831.

References

[1] H. Zhao, Y. Cun, X. Bai, et al., ACS Energy Lett. 7 (2022) 2060–2069.
[2] Y. Zhuang, X. Ren, X. Che, et al., Adv. Photonics 3 (2020) 014001.
[3] V. Diez Cabanes, C. Van Dyck, S. Osella, D. Cornil, J. Cornil, ACS Appl. Mater. Interfaces 13 (2021) 27737–27748.
[4] J.H. Zhang, H.P. Wang, L.Y. Zhang, et al., Chem. Sci. 11 (2020) 8885–8894.
[5] D. Li, Z. Feng, Y. Han, C. Chen, et al., Adv. Sci. 9 (2022) e2104790.
[6] Y. Yang, J. He, Z. He, G. Jiang, Adv. Opt. Mater. 9 (2020) 2001584.
[7] A. Abdollahi, H. Roghani-Mamaqani, B. Razavi, M. Salami-Kalajahi, ACS Nano 14 (2020) 14417–14492.
[8] Z. Li, Y. Dai, Z. Lu, et al., Eur. J. Org. Chem. 22 (2019) 3614–3621.
[9] M. Qin, Y. Huang, F. Li, Y. Song, J. Mater. Chem. C 3 (2015) 9265–9275.
[10] M. Natali, S. Giordani, Chem. Soc. Rev. 41 (2012) 4010–4029.
[11] L. Yang, Y. Li, H.F. Zhang, et al., Chin. Chem. Lett. 34 (2023) 108108.
[12] Y. Cai, Z. Guo, J. Chen, et al., J. Am. Chem. Soc. 138 (2016) 2219–2224.
[13] Y. Ai, Y. Fei, Z. Shu, et al., Chem. Eng. J. 450 (2022) 138390.
[14] W. Miao, S. Wang, M. Liu, Adv. Funct. Mater. 27 (2017) 1701368.
[15] K. Do, F.C. Muller, G. Muller, J. Phys. Chem. A 112 (2008) 6789–6793.
[16] M. Irie, T. Fukaminato, K. Matsuda, S. Kobatake, Chem. Rev. 114 (2014) 12174–12277.
[17] M. Irie, Chem. Rev. 100 (2000) 1685–1716.
[18] M. Li, H. Hu, B. Liu, et al., J. Am. Chem. Soc. 144 (2022) 20773–20784.
[19] H. Hayasaka, T. Miyashita, K. Tamura, K. Akagi, Adv. Funct. Mater. 20 (2010) 1243–1250.
[20] S. Du, X. Zhu, L. Zhang, M. Liu, ACS Appl. Mater. Interfaces 13 (2021) 15501–15508.
[21] Y. Kitagawa, S. Wada, M.D.J. Islam, et al., Chem. Commun. 3 (2020) 119.
[22] T. Harada, H. Tsumatori, K. Nishiyama, et al., Inorg. Chem. 51 (2012) 6476–6485.
[23] Z. Zhang, Y. Zhou, T. Gao, et al., Dalton Trans. 50 (2021) 4604–4612.
[24] Y. Zhang, Y. Zhou, T. Gao, P.F. Yan, H.F. Li, Chem. Commun. 56 (2020) 13213–13216.
[25] J. Zhang, Y. Zhou, Y. Yao, et al., J. Mater. Chem. C 8 (2020) 6788–6796.
[26] Y.R. Xia, A.Y. Hao, P.Y. Xing, Chin. Chem. Lett. 34 (2023) 107955.
[27] Z. Wang, A. Hao, P. Xing, Chin. Chem. Lett. 32 (2021) 1390–1396.
[28] N. Suzuki, S. Yoneyama, K. Shiba, T. Hasegawa, Y. Masuyama, Inorg. Chim. Acta 471 (2018) 355–363.
[29] K. Matsuda, M. Irie, Chem. Eur. J. 7 (2001) 3466–3473.
[30] Y. Zhou, Y. Yao, Z. Cheng, et al., Inorg. Chem. 59 (2020) 12850–12857.
[31] M. Yu, P. Zhang, L. Liu, et al., Adv. Opt. Mater. 9 (2021) 2101227.
[32] J. Ao, X. Fang, X. Miao, et al., Nat. Commun. 12 (2021) 3089.
[33] M. Latva, H. Takalo, V.M. Mukkala, et al., J. Lumin. 75 (1997) 149–169.
[34] Y. Huang, H.K. Bisoyi, S. Huang, et al., Angew. Chem. Int. Ed. 60 (2021) 11247–11251.
[35] Q. Zhang, D.H. Qu, H. Tian, Adv. Opt. Mater. 7 (2019) 1900033.
[36] L.E. MacKenzie, R. Pal, Nat. Rev. Chem. 5 (2020) 109–124.